

Article

Evaluation of Efficiency for Miniscale Thermoelectric Converter under the Influence of Electrical and Thermal Resistance of Contacts

Lyudmyla Vikhor ^{1,*}  and Maxim Kotsur ^{1,2}

¹ Institute of Thermoelectricity of the National Academy of Sciences and Ministry of Education and Science of Ukraine, 58029 Chernivtsi, Ukraine; m.kotsur@chnu.edu.ua

² Institute of Applied-Physics and Computer Sciences, Yuriy Fedkovych Chernivtsi National University, 58012 Chernivtsi, Ukraine

* Correspondence: vikhorl@ukr.net

Abstract: Mass-produced thermoelectric modules are mainly fabricated with Bi₂Te₃-based materials. Due to the limited world reserves and the high price of tellurium, it must be saved. The miniaturization of thermoelectric converters is one of the modern trends to diminish the use of tellurium, reduce the cost of modules and expand the range of their applications. The main disadvantage of miniature thermoelectric converters operating in cooling or generating modes is their low energy efficiency, caused by the effect of electrical and thermal resistances of contacts, interconnectors and insulating plates. We propose an improved method for evaluating the maximum efficiency that takes into consideration the impact of these unwanted resistances. This method can also be used to design the modules with the optimal structure for cooling and energy generation, and not only to study their performance. The effect of undesirable electrical and thermal resistances on the maximum efficiency of cooling and generating converters made of Bi₂Te₃-based materials is analyzed. It is shown that the efficiency of miniature modules can be significantly improved if these resistances are reduced to their rational values. The decrease in electrical contact resistance is the predominant factor. The rational values to which it is advisable to decrease the electrical contact resistance have been determined. In the development of miniscale module technology, it is necessary to focus on such rational contact resistance values.



Citation: Vikhor, L.; Kotsur, M. Evaluation of Efficiency for Miniscale Thermoelectric Converter under the Influence of Electrical and Thermal Resistance of Contacts. *Energies* **2023**, *16*, 4082. <https://doi.org/10.3390/en16104082>

Academic Editor: Mahmoud Bourouis

Received: 24 March 2023

Revised: 10 May 2023

Accepted: 11 May 2023

Published: 13 May 2023



Copyright: © 2023 by the authors. Licensee MDPI, Basel, Switzerland. This article is an open access article distributed under the terms and conditions of the Creative Commons Attribution (CC BY) license (<https://creativecommons.org/licenses/by/4.0/>).

Keywords: miniscale thermoelectric module; miniature thermoelectric converter; thermoelectric cooler; thermoelectric generator; maximum efficiency; electrical contact resistance; thermal resistance of insulating plate

1. Introduction

The practical application of thermoelectricity is currently constrained by the relatively high cost of thermoelectric energy converters. Figure 1a shows a diagram [1,2] of the growth in the market size of thermoelectric (TE) modules produced worldwide for the needs of thermoelectric power generation and cooling. The data are provided for the last 6 years with a prospect up to 2026. The market compound annual growth rate (CAGR) is about 9% [1,2]. Using this diagram and assuming that the average price of a standard TE module is near USD 15, we can easily estimate the annual production of modules in the world. The results of such a rough estimation are shown in Figure 1b. It can be seen that, at present, the production reaches about 54 million pieces per year. At the same time, the market potential is estimated at 6.2 billion pieces per year [3]. Consequently, the market for thermoelectric products, which are mainly cooling systems and converters of the waste heat into electricity, is provided for by less than 1% now. Therefore, the market needs are quite significant.

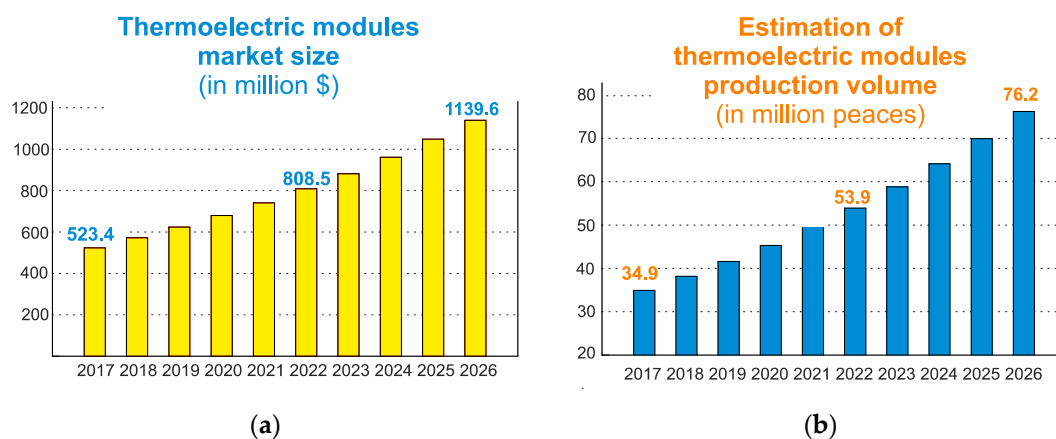


Figure 1. World market size (a) [1,2] and estimation of production volume (b) of thermoelectric modules.

It is generally known that commercial TE modules are mainly fabricated with Bi_2Te_3 -based materials. The main obstacle to increasing production is limited reserves, and hence the high price of tellurium. According to the estimates of the Energy Research Center (Great Britain), the world reserves of tellurium amount to 50 thousand tons only. The annual production of tellurium and its price in recent years are shown in Table 1 [4].

Table 1. Annual world production of tellurium and its price [4].

Year	2015	2016	2017	2018	2019	2020	2021	2022
Production, tons	400	400	420	460	520	562	610	640
Price, \$/kg	77	34	40	74	60	56	68	68

Therefore, today the average annual production of tellurium is more than 600 tons. Of this, 30% is spent on the needs of the thermoelectric industry [4], i.e., more than 180 tons per year. For a standard TE module, at least 5 g of tellurium is used. Consequently, the current level of tellurium production ensures today the manufacturing of approximately 36 million tellurium-containing modules per year, and the reserves of tellurium will suffice for 80 years. However, increasing the production of modules to at least 300 million pieces (which will correspond to 5% of the market demand only) will require 1500 tons of tellurium per year, and its annual production should be increased to at least 2000 tons. Then, the reserves of tellurium will last for 25 years only.

Therefore, for the development of the mass production of TE modules, it is necessary to reduce the use of tellurium drastically. There are several ways to do this. First of all, this is a search for new tellurium-free thermoelectric materials. Materials with high thermoelectric figures of merit and high mechanical properties are required.

No such materials have yet been proposed for thermoelectric coolers (TECs). Since the 1950s, cooling modules have been produced of Bi_2Te_3 -based materials, whose dimensionless figure of merit remains at the level of 1–1.2 [5]. The search for new tellurium-free materials with increased figures of merit does not give tangible positive results.

For thermoelectric generators (TEGs), a number of compounds are being investigated. Skutterudites and clathrates [6,7] are considered promising materials. Their optimization is predominantly focused on reducing their lattice thermal conductivity. The most attractive for practical applications are CoSb_3 -based skutterudites [8] whose crystal lattices are supplemented to reduce their thermal conductivity by rare-earth, alkaline-earth, alkali metals and other ions. The highest figures of merit, $ZT = 1.7$ [9] and $ZT = 1.9$ [10] at $T = 850$ K, were achieved for skutterudites $\text{Ba}_{0.08}\text{La}_{0.05}\text{Yb}_{0.04}\text{Co}_4\text{Sb}_{12}$ and $\text{Sr}_{0.09}\text{Ba}_{0.11}\text{Yb}_{0.05}\text{Co}_4\text{Sb}_{12.3}$, respectively. For clathrates, a high value of $ZT = 1.35$ [11] at $T = 900$ K was obtained for $\text{Ba}_8\text{Ga}_{16}\text{Ge}_{30}$ single-crystalline samples synthesized using the Czochralski method.

Intermetallic compounds Mg_2X ($X = Si, Ge, Sn$) are promising mid-temperature materials consisting of nontoxic and cheap elements. For solid solutions based on these compounds, such as $Mg_2Si_{1-x}Ge_x$ [12], $Mg_2Si_{1-x}Sn_x$ [13] and $Mg_2Sn_{1-x}Ge_x$ [14], ZT values in the range of 1.2–1.4 at near 800 K have been obtained for doped samples used as an n-type thermoelement in generator modules. For the p-type thermoelement, manganese silicides Mn_4Si_7 and $Mn_{11}Si_{19}$ with a figure of merit ZT in the range of 0.7–0.8 at 750 K are used [15,16]. Compounds such as Zn_4Sb_3 [17] and In_4Se_3 [18] are also promising for use in generator modules.

A lot of other compounds are being studied [8] for the middle range of operating temperatures from 500 K to 900 K and the high-temperature range from 900 K to 1300 K. For the low-temperature range from 300 K to 500 K, Bi_2Te_3 -based materials remain the most effective for thermoelectric generators. However, it should be noted that for new materials it is necessary to adapt and change the technology of mass production of TE modules.

There is another effective way to save world resources, in particular tellurium, and reduce the cost of TE modules. This is a reduction in the consumption of thermoelectric materials by miniaturization of thermoelements and the TE module as a whole. Miniaturization of thermoelectric converters (modules) is a modern trend in the improvement and expansion of their practical use [19].

A particularly important task is the miniaturization of modules for TECs, in the mass production of which materials other than Bi_2Te_3 -based compounds have not yet been used. Miniaturized cooling modules have a lot of important applications. Miniscale thermoelectric devices are used for cooling, controlling thermal conditions and stabilizing the temperature of electronic elements and systems. The main purpose of using a TEC is to remove heat and keep the electronic equipment at a normal operating temperature [20]. An additional task is to reduce the leakage current from electronic devices and the thermal noise from electrical components in order to improve the accuracy of devices [21]. An important application of TE modules is the spot cooling of electronic computer chips and their components [22–24]. Miniature TECs are used to control the temperature of the light-emitting diodes (LEDs) [25–27] and laser diodes [28,29] and to provide the required operating temperature of IR sensors [30–33].

Miniature TEGs are used in applications where a heat source is available and, in some cases, they can even replace batteries, for example, to power wireless sensors and autonomous circuitry placed in a harsh or remote environment [34,35]. These can be sensors for monitoring the operating condition of industrial processes or those in pipelines. TE converters are used in nuclear-based small-scale power sources for biomedical applications and implantable devices, such as pacemakers [36]. An example of such a Bi_2Te_3 -based converter made of 215 μm thick wafers is described in [37]. Miniscale TEGs are promising energy sources for wearable electronics and the “Internet of Things” devices [38–40]. Different wearable products with TEGs that use body heat have been developed, for example, a pulse-oximeter [41], a body-powered electroencephalogram system [42] and a wireless electrocardiography system inserted into a shirt [43,44]. Flexible TE modules with miniature thermoelements integrated into a fabric or silicon matrix [45] are more suitable for power generation from the human body [46–48]. Since miniscale TEGs usually operate at near room temperature conditions, Bi_2Te_3 -based materials are commonly used for such generators.

Thermoelectric converters are mechanically stable and highly reliable with a life cycle of up to 20 years. The main disadvantage here is their low energy efficiency. This study focuses on increasing the efficiency of miniscale TE modules for cooling and power generation. It should be noted that we identify the module with a length of thermoelements in the range from 500 μm to 200 μm as a miniature one. For the production of such modules, it is not necessary to change the existing technology. The conventional bulk technology with the manufacturing of thermoelements by thinning bulk materials is used [19,49].

2. Impact of Electrical and Thermal Contacts on Miniaturization of Thermoelectric Converters

It is well known that the efficiency of TE modules is mainly determined by the figure of merit $Z = \alpha^2\sigma/\kappa$, where α is the Seebeck coefficient, σ is the electrical conductivity and κ is the thermal conductivity of thermoelectric materials. However, it also depends on the electrical resistance of contacts at the boundaries between the semiconductor material of the legs and the metal connecting layers. A contact resistance is one of the main reasons for the fact that the thermoelectric properties of materials are not fully realized. The Joule heat releasing on the contacts reduces the efficiency of thermoelectric converters and leads to its dependence on the thermoelement length [50].

Figure 2 shows the dependences of efficiency (Figure 2a) and coefficient of performance (COP) (Figure 2b) on thermoelement length L for generating and cooling converters, respectively. The length L is indicated in Figure 3 below. These data have been calculated at a contact resistivity value of $r_c = 5 \times 10^{-6} \Omega \text{ cm}^2$ [51], which is considered typical for mass-produced modules made of Bi_2Te_3 -based materials.

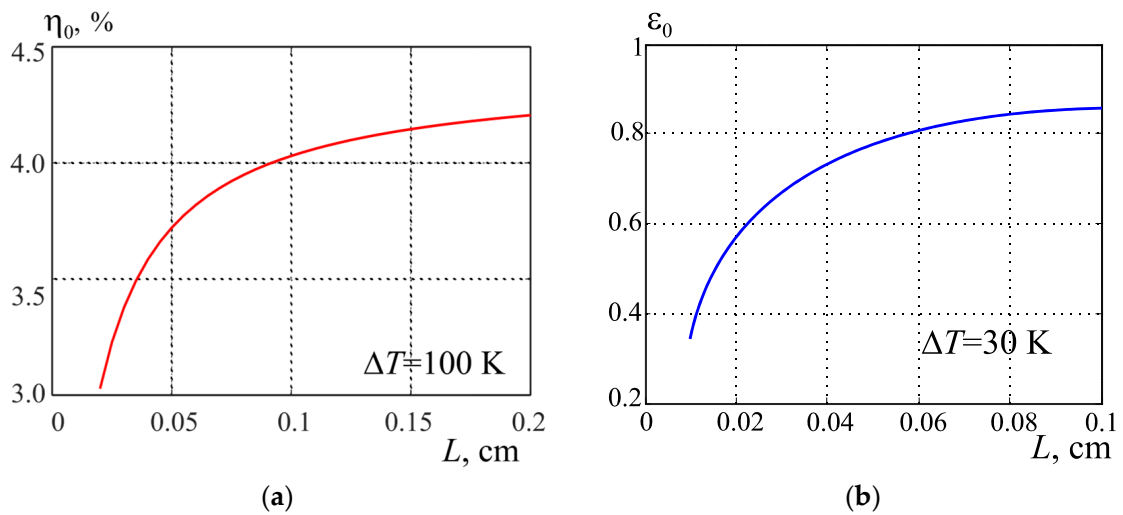


Figure 2. Dependences of maximum efficiency η_0 (a) and maximum COP ϵ_0 (b) on a thermoelement length L for the value of contact resistivity $r_c = 5 \times 10^{-6} \Omega \text{ cm}^2$.

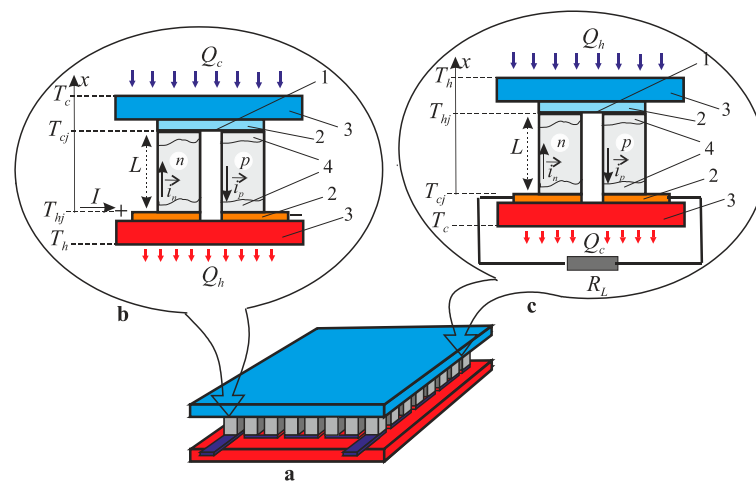


Figure 3. Schematic of TE module (a) and thermocouple converter in cooling mode (b) or power generation mode (c). 1—heat-absorbing thermocouple junction, 2—metallic interconnector, 3—insulating plate, 4—contact zone.

To calculate the maximum efficiency and COP, the classical formulae [52] have been used, which are given as

$$\eta_0 = \frac{T_h - T_c}{T_h} \frac{(M - 1)}{(M + T_c/T_h)}, \quad \varepsilon_0 = \frac{MT_c - T_h}{\Delta T(M + 1)}, \quad (1)$$

where, $M = \sqrt{1 + Z_{TE}(T_h + T_c)/2}$, $Z_{TE} = \alpha^2 / ((\rho + 2r_c/L)\kappa)$ is the figure of merit of the thermoelement that depends on the value of contact resistivity r_c . T_h and T_c are the hot side and cold side temperatures, respectively, and $\Delta T = T_h - T_c$, $\rho = 1/\sigma$ is the electrical resistivity of the thermoelectric material.

The influence of contact resistance on the efficiency and COP becomes more significant under the condition of thermoelement miniaturization when the thickness of the thermoelectric material–metal interfacial layer becomes comparable with the leg length. Attempts to create the miniature modules face a catastrophic decrease in the module efficiency. For example, for the cooling modules, it is desirable to reduce the thermoelement length from 0.1 cm to 0.01 cm. Under such conditions, the influence of contact resistivity, with a value of about $5 \times 10^{-6} \Omega \text{ cm}^2$, causes the decrease in COP at $\Delta T = 30 \text{ K}$ from approximately 0.8 to 0.1 (Figure 2), i.e., eightfold. Such modules, therefore, are no longer effective for practical applications.

It is possible to keep the energy efficiency value of miniature converters at a level sufficient for practical use by creating the contacts with significantly lower contact resistance. Therefore, the efforts of researchers are mainly focused on reducing the contact resistance [51,53–55].

Table 2 shows the theoretical and experimental results of studies of the contact resistivity between Bi_2Te_3 -based thermoelectric material (TEM) and anti-diffusion layers of metals, basically nickel, obtained in [51,56–59]. From Table 2, it follows that the improvement of contact technology enables reducing the contact resistivity to a value of about $(3\text{--}5) \times 10^{-7} \Omega \text{ cm}^2$.

Table 2. Resistivity of TEM–metal contact.

Contact	Features of Contact Technique	Contact Resistivity $r_c, \Omega \text{ cm}^2$	Reference
Calculation data			
p-type $\text{Bi}_2\text{Te}_3/\text{Ni}$	-	$(3.0\text{--}3.2) \times 10^{-6}$	[57]
n-type $\text{Bi}_2\text{Te}_{2.7}\text{Se}_{0.3}/\text{Ni}$, p-type $\text{Bi}_{0.5}\text{Sb}_{1.5}\text{Te}_3/\text{Ni}$	-	$(0.25\text{--}2.5) \times 10^{-6}$	[58]
Experimental data			
p-type BiSbTe/Ni	-	3.7×10^{-6}	[59]
n-type $\text{Bi}_2\text{Te}_{2.7}\text{Se}_{0.3}/$ anti-diffusion barrier	Fabrication of contact under the standard technology. Improved technology of surface treatment and cleaning.	2.74×10^{-6} 1.12×10^{-6}	[56]
p-type $\text{Bi}_{0.5}\text{Sb}_{1.5}\text{Te}_3/$ anti-diffusion barrier	Fabrication of contact under the standard technology. Improved technology of surface treatment and cleaning.	3.59×10^{-6} 1.3×10^{-6}	[56]
n-type $(\text{Bi,Sb})_2(\text{Se,Te})_3/\text{Ni}$	Processing and cleaning of the TEM surface. Ion implantation of impurities for increasing the carrier concentration at the TEM–metal boundary.	1.7×10^{-6} 4.5×10^{-7}	[51]
p-type $(\text{Bi,Sb})_2(\text{Se,Te})_3/\text{Ni}$	Processing and cleaning of the TEM surface. Ion implantation of impurities for increasing the carrier concentration at the TEM–metal boundary.	7.7×10^{-7} 2.7×10^{-7}	[51]

However, under miniaturization of thermoelectric legs, another factor is included in the process of reducing the efficiency, namely, the influence of thermal resistance of interconnectors and insulating plates in the module. Obviously, if the contact resistance approaches the minimum but technologically possible value, the role of thermal resistance becomes predominant, and a further decrease in contact resistance is not appropriate. Therefore, it is advisable to study the combined influence of electrical and thermal contacts

on the maximum efficiency value and to determine which of the resistances affects the efficiency more significantly with a decrease in the length of thermoelements for generators and coolers.

Approximate analytical methods for calculating the performances of TE converters considering electrical and thermal resistances are described in [49,60–63]. The heat balance equations at the hot and cold junctions of thermocouples are used. The main disadvantage of these methods is their limited accuracy due to simplifying assumptions, such as temperature independence of TE material parameters, disregarding the Thomson effect and others. More accurate one-dimensional [64–68] or three-dimensional [69–73] models and numerical methods are used to study the performance of cooling or generating converters taking into account the influence of various factors.

We offer a comprehensive one-dimensional theoretical model and a fairly accurate method that are suitable not only for analyzing the performance of TE converters, but also for designing the module with an optimal structure for TE coolers and generators.

3. Method for Designing and Calculating the Performance of TE Converter in Cooling and Generating Modes

3.1. Converter Physical Model

A schematic of a TE module for cooling or power generation is shown in Figure 3.

The module contains a number of thermocouples made of semiconductor n- and p-type legs, commonly referred to as thermoelements. Typically, the legs are connected in a series electrical circuit by metallic interconnectors and mounted between two insulating plates in parallel with respect to the heat flow.

If we pass an electric current I with the polarity, indicated in Figure 3b, and maintain the heat-liberating surface of the module at a temperature of T_h close to the ambient temperature, then the heat-absorbing surface will be cooled to a certain temperature of T_c . The module will operate in cooling mode.

If the absorbing junction is heated by a heat flow Q_h (Figure 3c) to a temperature of T_h , and the opposite junction is maintained at a temperature of T_c by the removing of heat Q_c , then due to the Seebeck effect, a thermo-EMF appears in a circuit. If the circuit is closed, the electric current passes and power is generated at the external load R_L . The module operates as a generator.

This schematic diagram is used to establish the appropriate mathematical relationships for the module's physical model. For simplicity, the heat flow is assumed to be one-dimensional. This assumption is reasonable since the interconnectors and insulating plates are usually thin and made of materials with good thermal conductivity. Therefore, the heat flow along the module surface due to local temperature gradients is neglected as it is usually compared to the heat flux across the thermoelements. The heat losses from the edges of the thermoelements and insulating plates are also neglected.

Moreover, as shown, for example, in [65], the results of calculating the module performance using the 3D approach differ, but only a little from the results obtained in the one-dimensional approximation.

3.2. Generating Converter

The efficiency of the generating converter is defined as the ratio

$$\eta = \frac{W}{Q_h}, \quad (2)$$

where, $W = Q_h - Q_c$ is electric power delivered to the load, Q_h is the heat power absorbed at the hot junction of the thermocouple, Q_c is the heat power liberated at the cold junction.

The values Q_h and Q_c should satisfy the energy balance equations, which are written as follows:

$$\begin{aligned} Q_h(R_{ins} + R_{con} + R_{hs}) &= (T_h - T_{hj}) \\ Q_c(R_{ins} + R_{con} + R_{cs}) &= (T_{cj} - T_c) \end{aligned} \quad (3)$$

where, T_{hj} and T_{cj} are the temperatures of the thermocouple’s hot and cold junctions, $R_{con} = \frac{l_{con}}{\kappa_{con}s_{con}}$ and $R_{ins} = \frac{l_{ins}}{\kappa_{ins}s_{ins}}$ are the thermal resistances of interconnector and insulating plate per one thermocouple, κ_{con} , κ_{ins} , l_{con} , l_{ins} , s_{con} and s_{ins} are their thermal conductivities, thickness and area, respectively. The thermal resistances $R_{hs} = \frac{1}{h_h s_{hs}}$ and $R_{cs} = \frac{1}{h_c s_{cs}}$ of the heat sinks on the hot and cold sides of the thermocouple can also be considered, where, h_h , h_c , s_{hs} and s_{cs} are their heat transfer coefficients and area, correspondingly.

Written in terms of heat flux densities, the expression (2) and Equation (3) become:

$$\eta = \frac{w}{q_h} \equiv \frac{q_h - q_c}{q_h}, \tag{4}$$

$$\begin{aligned} q_h R_{th} &= (T_h - T_{hj}) \\ q_c R_{tc} &= (T_{cj} - T_c) \end{aligned} \tag{5}$$

where, $R_{th} = \frac{l_{con}}{\kappa_{con}K_{con}} + \frac{l_{ins}}{\kappa_{ins}K_{ins}} + \frac{1}{h_h K_{hs}}$ and $R_{tc} = \frac{l_{con}}{\kappa_{con}K_{con}} + \frac{l_{ins}}{\kappa_{ins}K_{ins}} + \frac{1}{h_c K_{cs}}$. $K_{con} = \frac{s_{con}}{s_n + s_p}$, $K_{ins} = \frac{s_{ins}}{s_n + s_p}$, $K_{hs} = \frac{s_{hs}}{s_n + s_p}$ and $K_{cs} = \frac{s_{cs}}{s_n + s_p}$ are the fill factors of the interconnector, insulating plate and hot and cold heat sinks, respectively. $q_h = \frac{Q_h}{s_n + s_p}$ and $q_c = \frac{Q_c}{s_n + s_p}$ denote the densities of heat absorbed at the hot junction and rejected at the cold junction of the thermocouple, respectively. $w = q_h - q_c$ is a power density and s_n and s_p are the cross-sectional areas of n- and p-type legs, respectively.

To determine the heat flux densities q_h , q_c , we use the one-dimensional equation of heat flow in the thermoelectric leg at a steady state, which has the following form [50,52]:

$$\frac{d}{dx} \kappa \frac{dT}{dx} + \frac{i^2}{\sigma} - T \frac{d\alpha}{dT} i \frac{dT}{dx} = 0, \tag{6}$$

where, $i \equiv \left| \vec{i} \right| = I/s$ is a current density. In this equation, the thermoelectric material properties, namely, the Seebeck coefficient $\alpha(T)$, the electrical conductivity $\sigma(T)$ and the thermal conductivity $\kappa(T)$ are temperature dependent. The last term on the left-hand-side of Equation (6) represents the Thomson effect which, as shown in [69], can affect the performances of the converters.

To calculate the temperature $T(x)$ and heat flux $q(x)$ distributions in the n- and p-type legs of the thermocouple, a new variable $q = -\kappa \frac{dT}{dx} + \alpha iT$ is used to write the two second-order differential Equation (6) for legs in the form of a system of four first-order equations as follows:

$$\begin{aligned} \frac{dT_n}{dx} &= -\frac{q_n}{\kappa_n} - \frac{\alpha_n}{\kappa_n} i_n T_n; & \frac{dT_p}{dx} &= -\frac{q_p}{\kappa_p} - \frac{\alpha_p}{\kappa_p} i_p T_p \\ \frac{dq_n}{dx} &= \frac{\alpha_n^2}{\kappa_n} i_n^2 T_n + \frac{\alpha_n}{\kappa_n} i_n q_n + \frac{i_n^2}{\sigma_n}; & \frac{dq_p}{dx} &= \frac{\alpha_p^2}{\kappa_p} i_p^2 T_p + \frac{\alpha_p}{\kappa_p} i_p q_p + \frac{i_p^2}{\sigma_p} \end{aligned} \tag{7}$$

where, $\alpha_n = |\alpha_n|$. In system (7), it was taken into consideration that the equality $\alpha \vec{i} = -|\alpha i|$ is valid for both n- and p-type legs since a change in the type of conductivity in a thermocouple occurs simultaneously with a change in the direction of the current density vector (Figure 3c).

The solution of system (7) at given current densities i_n and i_p under boundary conditions

$$T_n(L) = T_p(L) = T_{hj}; \quad T_n(0) = T_p(0) = T_{cj} \tag{8}$$

enables determining the heat fluxes q_h and q_c according to the following formulae:

$$\begin{aligned} q_h &= -\left[q_n(L) + q_p(L) + i_n^2 r_c + i_p^2 r_c + q_{con} \right] \\ q_c &= -\left[q_n(0) + q_p(0) - i_n^2 r_c - i_p^2 r_c - q_{con} \right] \end{aligned} \tag{9}$$

These formulae take into account the release of Joule heat due to contact resistance r_c at the junctions of the thermocouple. The liberation of Joule heat in the metallic interconnector is also considered. Using the expression for interconnector resistance obtained in [50], the density q_{con} of this heat can be approximated as follows:

$$q_{con} = \frac{\rho_{con}}{l_{con}} (K_{con} - 2/3) I (i_n + i_p), \tag{10}$$

where, ρ_{con} is the resistivity of the connecting material.

Consequently, using the nonlinear system of Equation (5) to find the unknown temperatures T_{hj} and T_{cj} and the solution of the boundary value problem (7) and (8) to calculate q_h and q_c (9), it is possible to determine the efficiency (4) for the given current densities i_n and i_p . The variation of i_n and i_p makes it possible to find the optimal current densities $i_{n\ opt}$ and $i_{p\ opt}$, at which the efficiency takes the maximum value η_{max} .

The initial data for solving such an optimization problem and for designing a generating module are temperatures T_h and T_c , the required electric power W_L and voltage V_L on the external load. Therefore, the current I in the closed circuit is also given and is equal to $I = W_L / V_L$. The temperature dependences of materials parameters $\alpha_{n,p}(T)$, $\sigma_{n,p}(T)$ and $\kappa_{n,p}(T)$, leg length, contact resistance, thicknesses and filling factors of the interconnector, insulating plate and heat sinks should also be specified. Then, the optimal cross-sectional areas of the n- and p-type legs are calculated using the ratio $s_{n\ opt} = I / i_{n\ opt}$, $s_{p\ opt} = I / i_{p\ opt}$ and the number of thermocouples providing the required power W_L is determined by the following formula: $n = \frac{W_L}{(s_{n\ opt} + s_{p\ opt})(q_h - q_c)}$. Obviously, numerical methods are used for calculations.

It should be noted that, in order to design a module with the same cross-sectional area ($s_n = s_p$) of the legs, it is necessary to put $i_n = i_p$ for calculations.

3.3. Cooling Converter

The energy efficiency of the cooling module is determined by the COP ϵ , which is given by

$$\epsilon = \frac{Q_c}{W}, \tag{11}$$

where, $W = Q_h - Q_c$ is the consumed electric power, Q_c is the heat power absorbed at the cold junction of a thermocouple and Q_h is the heat power liberated at the hot junction.

The values Q_c and Q_h should satisfy the energy balance equations, which are written as follows:

$$\begin{aligned} Q_c(R_{ins} + R_{con} + R_{cs}) &= (T_c - T_{cj}) \\ Q_h(R_{ins} + R_{con} + R_{hs}) &= (T_{hj} - T_h) \end{aligned} \tag{12}$$

Written in terms of heat flux densities, the expression (11) for the COP and Equation (12) become:

$$\epsilon = \frac{q_c}{q_h - q_c}, \tag{13}$$

$$\begin{aligned} q_c R_{tc} &= (T_c - T_{cj}) \\ q_h R_{th} &= (T_{hj} - T_h) \end{aligned} \tag{14}$$

To determine the heat flux densities q_c and q_h , we solve the system of differential Equation (7) with the following boundary conditions:

$$T_n(0) = T_p(0) = T_{hj}; \quad T_n(L) = T_p(L) = T_{cj}, \tag{15}$$

and use the relations:

$$\begin{aligned} q_c &= - \left[q_n(L) + q_p(L) + i_n^2 r_c + i_p^2 r_c + q_{con} \right] \\ q_h &= - \left[q_n(0) + q_p(0) - i_n^2 r_c - i_p^2 r_c - q_{con} \right] \end{aligned} \tag{16}$$

So, solving the system of Equation (14) and the boundary value problems (7)–(15) for given current densities i_n and i_p , we find the heat flux densities q_c and q_h (9) using formulae (16) and determine the COP (13). The variation of i_n and i_p makes it possible to find the optimal current densities $i_{n\ opt}$ and $i_{p\ opt}$, at which the COP takes the maximum value ε_{max} .

The described method is used for designing of the cooling module with the maximum COP at temperature difference $\Delta T = T_h - T_c$ considering the electrical and thermal resistances of contacts, interconnectors, insulating plates and heat sinks. For a given value of current I , the optimal cross-section areas of n- and p-type legs are calculated using the ratio $s_{n\ opt} = I/i_{n\ opt}$, $s_{p\ opt} = I/i_{p\ opt}$ and the number of thermocouples providing the required cooling capacity Q_m of the module is determined as follows: $n = Q_m / (q_c(s_{n\ opt} + s_{p\ opt}))$.

3.4. Algorithm for Designing and Calculating the Performance of TE Converter

To design and calculate the performance of TE converters, a special iterative algorithm was developed, which consists of the following:

1. We set the initial values of the current densities $i_n^{(0)} = i_p^{(0)} \equiv i^{(0)}$ and the initial values of $T_{cj}^{(0)}$, $T_{hj}^{(0)}$, close to the values of T_c and T_h . To calculate $i^{(0)}$, we used approximate classical expressions [52] for the optimal current density, which are given as follows: $i_{\eta}^{(0)} = \frac{\alpha\Delta T}{\rho L(M+1)}$ for the generating converter or $i_{\varepsilon}^{(0)} = \frac{\alpha\Delta T}{\rho L(M-1)}$ for the cooling mode, where, $\alpha = \bar{\alpha}_n + \bar{\alpha}_p$, $\rho = \bar{\rho}_n + \bar{\rho}_p + 4r_c/L$, $\bar{\alpha}_n$, $\bar{\alpha}_p$, $\bar{\rho}_n$, $\bar{\rho}_p$ are the average values of parameters in the temperature range ΔT .
2. We apply the Newton iteration method to solve the system of Equations (5) or (14) for the generating or cooling converter, respectively, and find the next approximation for the temperatures $T_{cj}^{(i)}$, $T_{hj}^{(i)}$.
3. Within each Newton iteration, we solve the boundary value problem (7) and (8) or (7)–(15) and calculate the heat flux densities q_c and q_h according to Formula (9) or (16). For this, we use the finite element method in combination with the shooting method.
4. For each Newton iteration, we determine η or ε by Formula (4) or (11), respectively, and vary current densities i_n and i_p using the gradient method until finding η_{max} or ε_{max} .
5. Newton's iterative process is repeated until the specified accuracy is reached in solving the system of Equations (5) or (14).

Such an algorithm was implemented in MATLAB.

4. Results and Discussion

Our goal was to investigate the effect of electrical and thermal resistances of contacts, interconnectors and insulating plates on the energy efficiency of TE converters with the leg length from 0.2 cm to 0.02 cm. The maximum COP and maximum efficiency were calculated for modules made of Bi₂Te₃-based materials. The samples of n- and p-type Bi₂Te₃-based alloys for cooling and generating modules were grown at the Institute of Thermoelectricity (Ukraine) by the vertical zone-melting technique and their thermoelectric properties were measured using the methods and equipment developed herein [74,75]. The measured temperature dependences of the Seebeck coefficient $\alpha(T)$, the electrical conductivity $\sigma(T)$ and the thermal conductivity $\kappa(T)$ are shown in Figure 4. These dependences were approximated by polynomials and used for the COP and efficiency calculation. The composition of Bi₂Te₃-based alloys for cooling modules differs from the composition for generator modules. The generator materials are chosen in such a way that the maximum of the Seebeck coefficient is in the hot temperature range from 400 K to 500 K (Figure 4a). Figure 4d shows the temperature dependences of material figure of merit Z . Obviously, the alloys used for cooling modules have a maximum Z value in the temperature range from 250 K to 300 K. For generator materials, the maximum Z is shifted to the range of 300 K–350 K, and the Z value at temperatures of 400 K–450 K is higher compared to cooling materials.

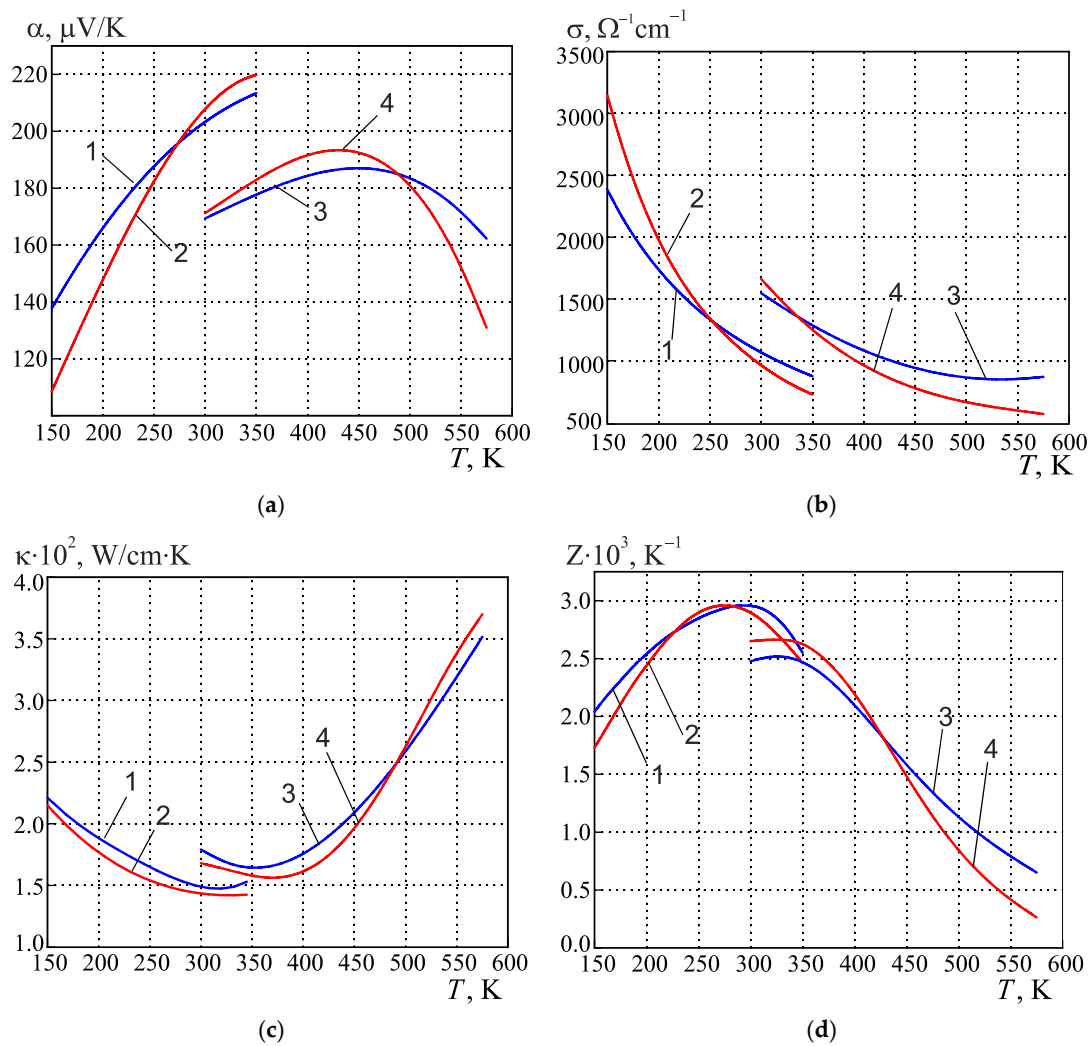


Figure 4. Temperature dependences of the Seebeck coefficient α (a), the electrical conductivity σ (b), the thermal conductivity κ (c) and the figure of merit Z (d) of materials for cooling modules: 1—n-type $\text{Bi}_2\text{Te}_{2.7}\text{Se}_{0.3}$, 2—p-type $\text{Bi}_{0.5}\text{Sb}_{1.5}\text{Te}_3$ and alloys used for generating converters: 3—n-type $(\text{Bi}_2\text{Te}_3)_{0.90}(\text{Sb}_2\text{Te}_3)_{0.05}(\text{Sb}_2\text{Se}_3)_{0.05}$, 4—p-type $(\text{Bi}_2\text{Te}_3)_{0.25}(\text{Sb}_2\text{Te}_3)_{0.72}(\text{Sb}_2\text{Se}_3)_{0.03}$.

Calculations were carried out for modules with the same cross-sectional area ($s_n = s_p$) of the legs connected by copper interconnectors. Three ceramic materials were considered for insulating plates, namely, aluminum oxide Al_2O_3 , aluminum nitride AlN and pressed diamond powder. The initial data for calculating the efficiency and COP are given in Table 3.

Table 3. Value of parameters used for calculation.

Parameter	Value
Leg length L , cm	0.02–0.2
Ratio $K_{con} = s_{con}/2s$	1.25
Ratio $K_{ins} = s_{ins}/2s$	2.25
Thickness of the insulating plate l_{ins} , cm	0.02
Thickness of the copper interconnector l_{con} , cm	0.02
Current in a circuit I , A	1.0
Thermal conductivity of insulating plate materials κ_{ins} , W/cm K:	
Al_2O_3	0.24
AlN	1.25
Pressed diamond powder	10.0

4.1. Cooling Converter

The dependences of the maximum COP ε_{max} on a thermoelement length, calculated for temperature differences across the modules of 30 K and 50 K, are shown in Figure 5.

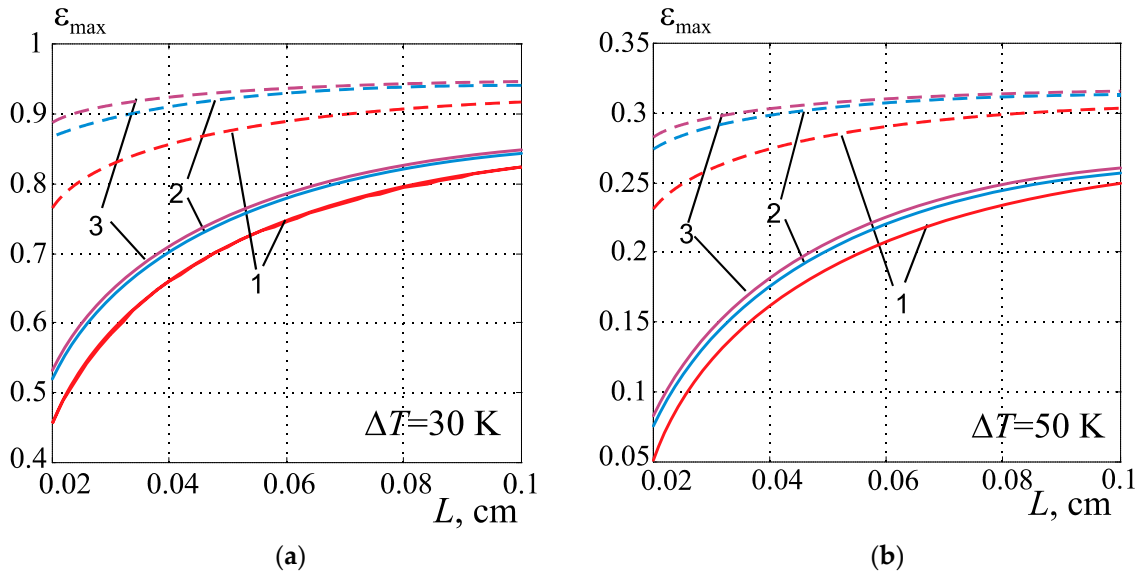


Figure 5. Dependences of the maximum COP ε_{max} on the leg length L . Contact resistance: $r_c = 5 \times 10^{-6} \Omega \text{ cm}^2$ (solid lines), $r_c = 10^{-7} \Omega \text{ cm}^2$ (dashed lines). Insulating plates: 1—Al₂O₃, 2—AlN and 3—pressed diamond powder. Temperature difference: $\Delta T = 30$ K (a) and $\Delta T = 50$ K (b). $T_h = 300$ K.

To analyze the impact of electrical contact resistance on the maximum COP, calculations were performed for two values of resistivity r_c , namely, for the value $r_c = 5 \times 10^{-6} \Omega \text{ cm}^2$, which is considered as typical for commercial TE modules [51], and for the minimum value $r_c = 10^{-7} \Omega \text{ cm}^2$. As shown in [58,76], such minimum contact resistance is caused by a potential barrier at the boundary between the TEM and the nickel anti-diffusion layer. As it follows from the data in Table 2, the lowest value of contact resistivity measured experimentally is close to $10^{-7} \Omega \text{ cm}^2$.

The effect of the thermal resistance of interconnectors and insulating plates results in the dependence of ε_{max} on a thermoelement length for both the minimum (dashed lines in Figure 5) and the typical (solid lines in Figure 5) values of contact resistance. Reducing the leg length of module leads to a decrease in the COP, which is especially sharp if the length is less than 0.05 cm and the contact resistance is high.

Thermal resistance evokes the unwanted temperature drops δT across the interconnectors and insulating plates (Figure 6), which for modules with miniscale thermoelements, are the greater the shorter the leg.

Obviously, δT_h across the heat-releasing (solid lines in Figure 6) insulating plate is significantly greater than the drop δT_c across the heat-absorbing one (dashed lines in Figure 6). The larger the temperature difference across the module and the thermal resistance of the insulating plates, the greater δT . For example, for modules with a leg length of 0.02 cm and insulating plates made of Al₂O₃, δT_h reaches a value of 3.5 K (Figure 6b) for a temperature difference across the module of $\Delta T = 50$ K. Accordingly, the temperature of heat-releasing junctions of thermocouples increases by the same value, thus causing a reduction of the COP.

An improvement in the COP can be obtained by decreasing the thermal resistance of insulating plates. This is achieved by reducing the plate thickness and using ceramics with high thermal conductivity, such as AlN or pressed diamond powder. In particular, for insulating plates made of AlN, the temperature drop δT_h has a value of less than 1 K instead of 3.5 K (Figure 6). In general, the temperature losses δT_h for miniature modules

with Al_2O_3 insulating plates are about 3.5 times or 8 times higher than δT_h for modules with AlN or pressed diamond ceramics, respectively.

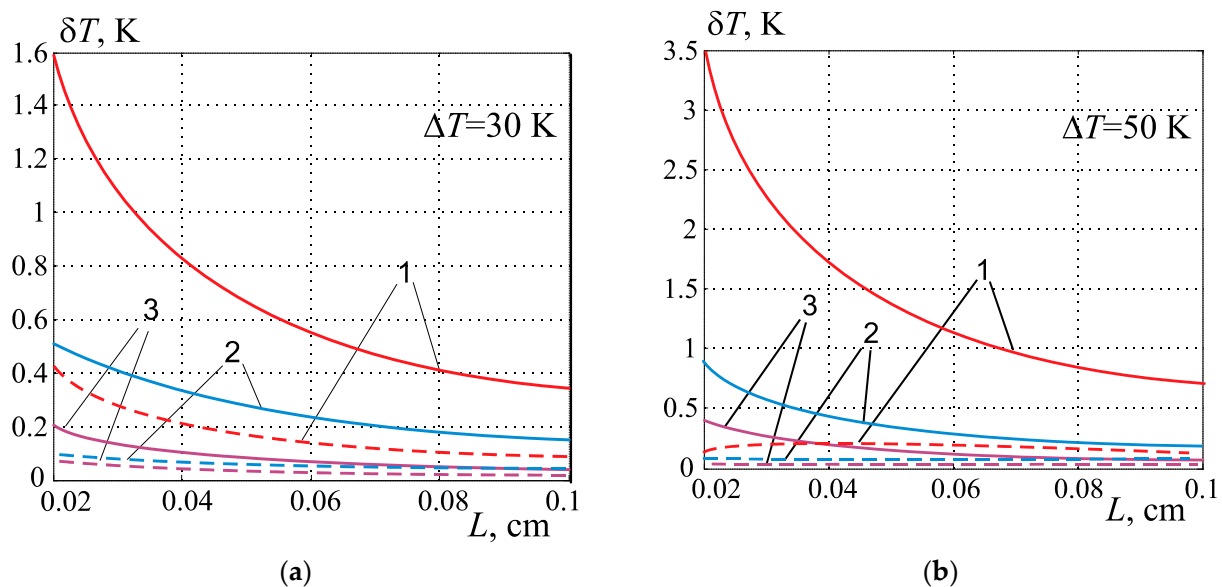


Figure 6. Dependences of temperature drop δT across the heat-releasing (solid lines) and heat-absorbing (dashed lines) insulating plates on the leg length L . $r_c = 5 \times 10^{-6} \Omega \text{ cm}^2$. Insulating plates: 1— Al_2O_3 , 2—AlN and 3—pressed diamond powder. $\Delta T = 30$ K (a), $\Delta T = 50$ K (b), $T_h = 300$ K.

However, the data in Figure 5 show that the COP of modules with diamond insulating plates does not differ significantly from the COP of modules with AlN ceramics. Therefore, it is impractical to use materials with a thermal conductivity greater than that of aluminum nitride for insulating plates. In particular, using an expensive diamond ceramic is not reasonable. However, when choosing the material for insulating plates and plate thickness, the mechanical properties of the ceramics must be also taken into account.

We also studied the effect of interconnector electrical resistance on the COP of miniature modules. The optimal supply current for such modules usually does not exceed 3 A [49], and the Joule heat that is released in the interconnector has little effect on the COP.

Figure 7 shows the dependences of the COP ε_{max} on the temperature difference ΔT across the miniscale module with the leg length of $L = 0.02$ cm. The COP has been calculated for different electrical and thermal resistances of contacts and insulating plates. This figure also represents the dependence $\varepsilon_0(\Delta T)$, corresponding to the ideal model of the module (without undesirable electrical and thermal resistances). It can be seen that the COP ε_{max} approaches the value ε_0 of an ideal model, only if the contact electrical resistance is minimal and the insulating plates are made of materials with high thermal conductivity. Otherwise, ε_{max} of the miniature module is 2–6 times less than the value of ε_0 . This result follows from the data of calculating the ratio $\varepsilon_0/\varepsilon_{max}$ presented in Table 4.

The analysis of these data also shows that a significant improvement in the COP of miniscale modules can be achieved by decreasing the electrical contact resistance to its rational value. An increase in the COP by reducing the thermal resistance of insulating plates is less noticeable.

To determine the rational values, the dependences of the maximum COP on the contact resistivity were calculated and analyzed. The results are shown in Figure 8 for the temperature differences of $\Delta T = 10$ K and $\Delta T = 50$ K. The data were calculated for cooling converters with a typical leg length of 0.1 cm and with miniature legs of 0.02 cm. Modules with the insulating plates of both Al_2O_3 and AlN materials were considered.

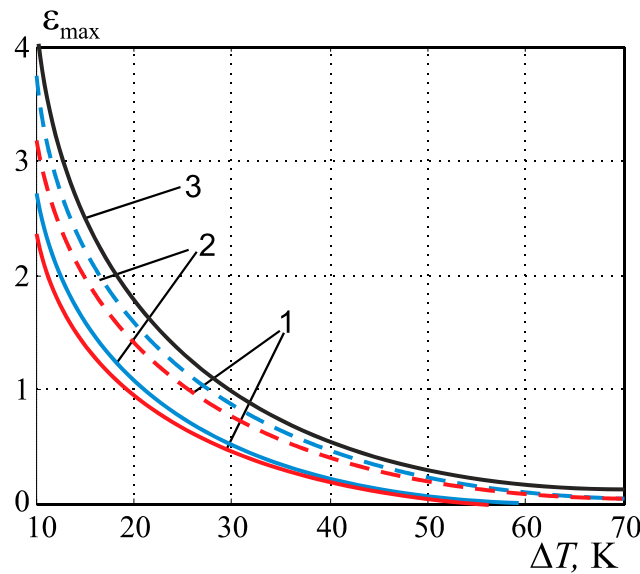


Figure 7. Dependences of the maximum COP ϵ_{max} on the temperature difference ΔT , at $T_h = 300$ K. $L = 0.02$ cm, $r_c = 5 \times 10^{-6} \Omega \text{ cm}^2$ (solid lines), $r_c = 10^{-7} \Omega \text{ cm}^2$ (dashed lines), insulating plates: 1— Al_2O_3 , 2— AlN . 3—dependence $\epsilon_0(\Delta T)$ for the ideal model of module.

Table 4. Ratio $\epsilon_0/\epsilon_{max}$ of ideal module COP ϵ_0 to real module COP ϵ_{max} in dependence of thermoelement length.

Leg Length L , cm	$\epsilon_0/\epsilon_{max}$ $r_c = 10^{-7} \Omega \text{ cm}^2$, AlN Insulating Plates	$\epsilon_0/\epsilon_{max}$ $r_c = 10^{-7} \Omega \text{ cm}^2$, Al_2O_3 Insulating Plates	$\epsilon_0/\epsilon_{max}$ $r_c = 5 \times 10^{-6} \Omega \text{ cm}^2$, AlN Insulating Plates	$\epsilon_0/\epsilon_{max}$ $r_c = 5 \times 10^{-6} \Omega \text{ cm}^2$, Al_2O_3 Insulating Plates
Temperature difference across a module $\Delta T = 10$ K, $\epsilon_0 = 4.149$				
0.1	1.02	1.06	1.10	1.14
0.05	1.04	1.12	1.21	1.29
0.02	1.11	1.30	1.54	1.77
Temperature difference across a module $\Delta T = 30$ K, $\epsilon_0 = 0.961$				
0.1	1.02	1.05	1.14	1.17
0.05	1.04	1.10	1.29	1.35
0.02	1.11	1.26	1.85	2.11
Temperature difference across a module $\Delta T = 50$ K, $\epsilon_0 = 0.324$				
0.1	1.03	1.07	1.25	1.29
0.05	1.07	1.14	1.59	1.72
0.02	1.18	1.40	4.18	6.47

The value of the contact resistance strongly affects the COP. The lower the contact resistance, the higher the COP of converter. This dependence is more intense for a converter with miniature legs. In particular, for a converter with a thermoelement length of 0.02 cm, the COP at $\Delta T = 50$ K decreases to zero (Figure 8b) if the contact resistivity exceeds the value of $5 \cdot 10^{-6} \Omega \cdot \text{cm}^2$. This means that the maximum temperature difference of such a converter reaches only 50 K.

However, the data in Figure 8 show that for a converter with a certain length of thermoelements, there is a rational value $r_{c \text{ opt}}$ of the contact resistivity, such that for $r_c < r_{c \text{ opt}}$ the increase in the COP becomes insignificant, namely, not exceeding 5%. The results of computer calculations have shown that the rational value of $r_{c \text{ opt}}$ depends only on the length of the converter legs and does not depend either on the temperature drop in the converter or on the thermal resistance of the insulating plates. To determine the value of $r_{c \text{ opt}}$, we calculated the dependences $\epsilon_{max}(r_c)$ for converters with different leg lengths.

They are shown in Figure 9. It can be seen that for each length there is its own value $r_{c\ opt}$ of contact resistivity, such that for $r_c < r_{c\ opt}$ the dependences $\epsilon_{max}(r_c)$ go into saturation. The rational values $r_{c\ opt}$ have been defined for cooling converters with different leg lengths and are given in Table 5.

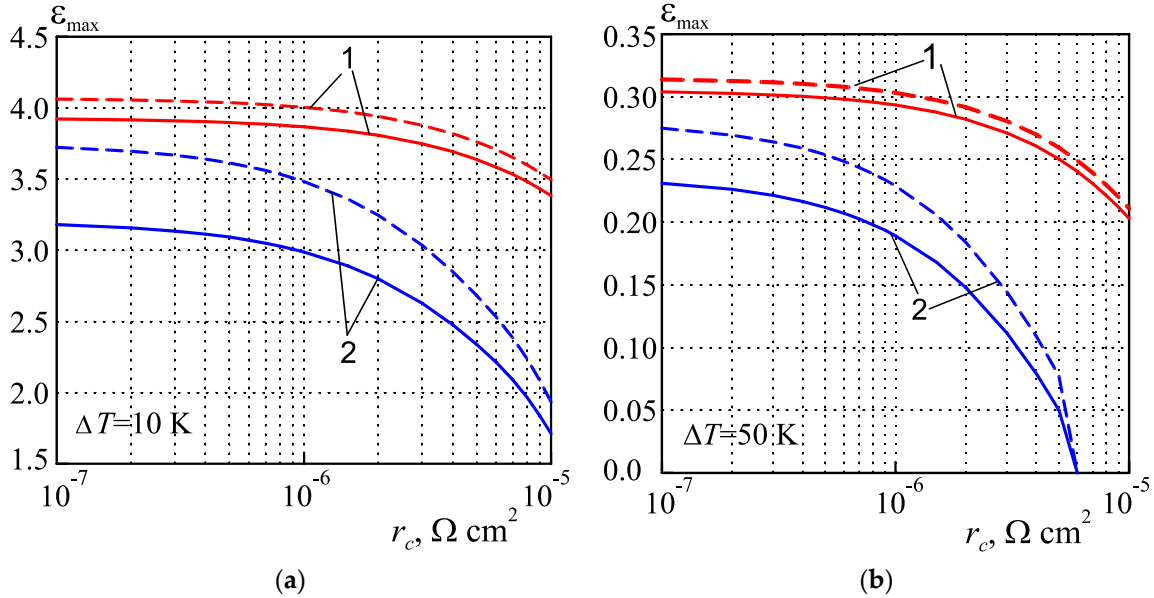


Figure 8. Dependences of the COP ϵ_{max} on the contact resistivity r_c for temperature differences $\Delta T = 10 \text{ K}$ (a) and $\Delta T = 50 \text{ K}$ (b). 1—leg length $L = 0.1 \text{ cm}$, 2— $L = 0.02 \text{ cm}$; insulating plates made of Al_2O_3 (solid lines) and AlN (dashed lines).

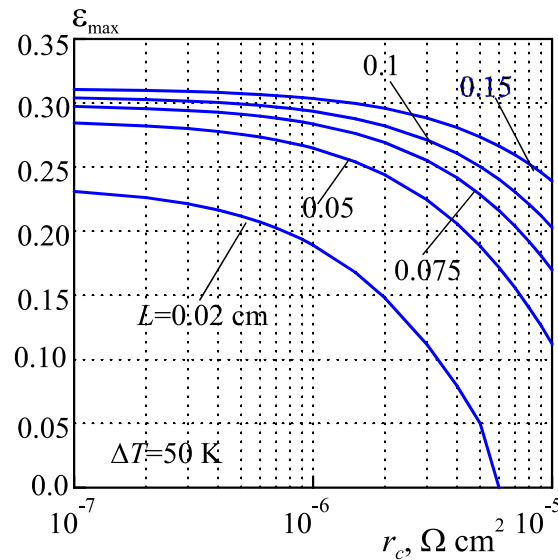


Figure 9. Dependences of COP ϵ_{max} on the contact resistance r_c for different leg lengths L . $\Delta T = 50 \text{ K}$, insulating plates made of Al_2O_3 .

Table 5. The rational values of the contact resistivity for cooling converters with different leg lengths.

Thermoelement length $L, \text{ cm}$	0.15	0.1	0.075	0.05	0.02
Rational contact resistivity $r_{c\ opt}, \Omega \cdot \text{cm}^2$	$2 \cdot 10^{-6}$	10^{-6}	$9 \cdot 10^{-7}$	$7 \cdot 10^{-7}$	$3 \cdot 10^{-7}$

It is necessary to focus on such rational values of contact resistance in the development of technology for creating the junction between Bi₂Te₃-based material and anti-diffusion metal for cooling modules, especially for the modules with miniscale thermoelements.

4.2. Generating Converter

The influence of electrical and thermal resistances of contacts, interconnectors and insulating plates on the efficiency and power density was studied for generating converters. Dependences of the maximum efficiency η_{\max} and power density w on the leg length, calculated for temperature drops of 25 K and 100 K on the generating module are shown in Figure 10. Reducing the length of the thermoelements leads to a decrease in efficiency, which is especially sharp if the length is less than 0.1 cm and the contact resistance is high. It is obvious that with a decrease in the leg length, the density of the generated power increases. This testifies to the absolute advantage of converters with miniature thermoelements. However, unwanted electrical and thermal resistances significantly affect this advantage, reducing the power density.

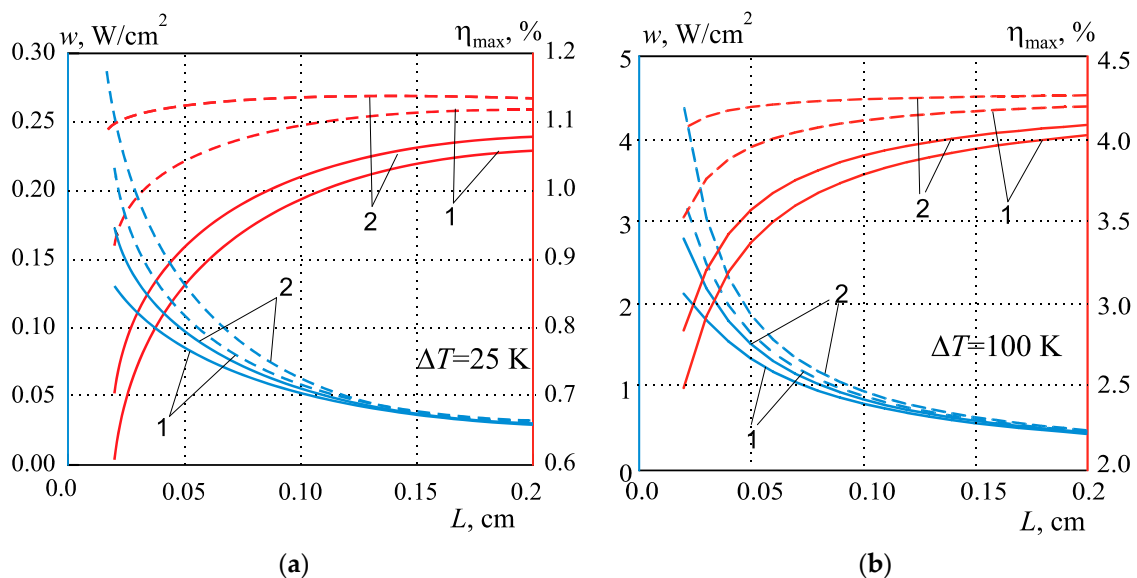


Figure 10. Dependences of the maximum efficiency η_{\max} and power density w on the leg length L . Contact resistance: $r_c = 5 \times 10^{-6} \Omega \text{ cm}^2$ (solid lines), $r_c = 10^{-7} \Omega \text{ cm}^2$ (dashed lines). Insulating plates: 1—Al₂O₃, 2—AlN. Temperature difference: $\Delta T = 25$ K (a), $\Delta T = 100$ K (b). $T_c = 300$ K.

Thermal resistance causes a temperature drop δT across the insulating plates, which depends on the leg length and the temperature difference across the converter, as shown in Figure 11. In a module with miniature legs, the drop δT can reach a high value. For example, for a module with insulating plates made of Al₂O₃, $\delta T = 8.5$ K (Figure 11). Because of the generating module $\delta T_h \approx \delta T_c$, the losses of the temperature difference across the module, in this case, are about 17 K, which results in a significant reduction in efficiency.

We also investigated the influence of copper interconnectors on the performance of the generating converter. Their thermal resistance actually does not affect the efficiency. However, their electrical resistance can affect the efficiency if the module is designed for a load with a large input current. The dependence of efficiency on the current in the thermoelectric circuit is shown in Figure 12. If the current is low, the Joule heat released in the interconnector has little effect on the efficiency. However, if the current exceeds a certain critical value of I_{cr} , the efficiency decreases sharply. The value I_{cr} depends on the temperature drop across the converter and does not depend on the leg length. In order to avoid a decrease in efficiency at high currents, it is enough to increase the thickness of the interconnector. This is confirmed by the dependences $\eta_{\max}(I_{con})$ at the high currents shown in Figure 13.

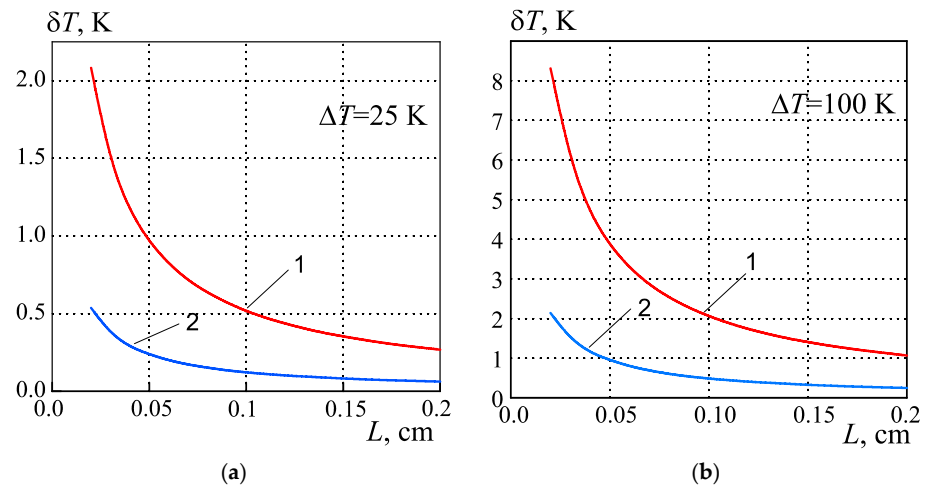


Figure 11. Dependences of temperature drop δT across the insulating plate on the leg length L . $r_c = 5 \times 10^{-6} \Omega \text{ cm}^2$, insulating plate: 1—Al₂O₃, 2—AlN, $\Delta T = 25$ K (a), $\Delta T = 100$ K (b), $T_c = 300$ K.

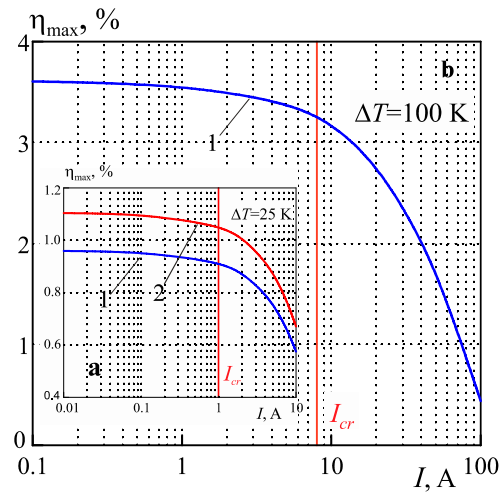


Figure 12. Dependences of the efficiency η_{max} on the current I in thermoelectric circuit. $r_c = 5 \times 10^{-6} \Omega \text{ cm}^2$, AlN insulating plate, leg length 1— $L = 0.05$ cm, 2— $L = 0.15$ cm. $\Delta T = 25$ K (a), $\Delta T = 100$ K (b).

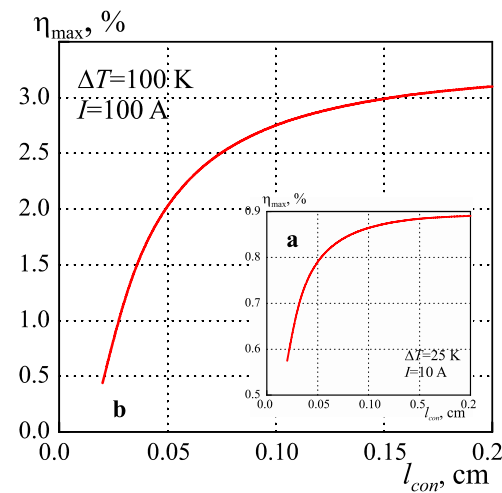


Figure 13. Dependences of the efficiency η_{max} on the thickness of interconnector l_{con} . AlN insulating plates, $r_c = 5 \times 10^{-6} \Omega \text{ cm}^2$, $L = 0.05$ cm. $\Delta T = 25$ K and $I = 10$ A (a), $\Delta T = 100$ K and $I = 100$ A (b). $T_c = 300$ K.

Dependences of maximum efficiency η_{max} on the temperature drop ΔT across the module with the miniature legs are shown in Figure 14. Dependence $\eta_0(\Delta T)$ for the ideal module model (without undesirable electrical and thermal resistances) is also given. The calculated ratio η_0/η_{max} is presented in Table 6. The ratio w_0/w of power density values is also shown in this Table.

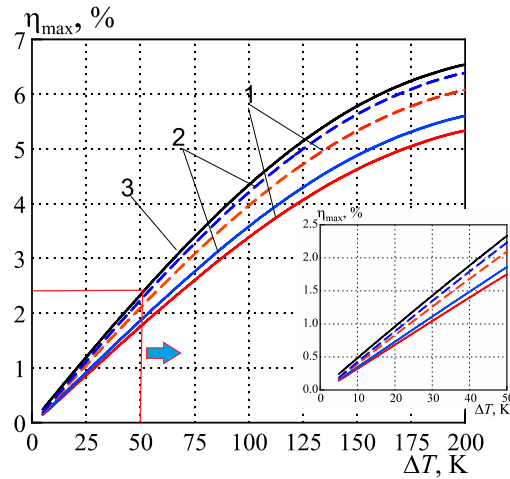


Figure 14. Dependences of maximum efficiency η_{max} on the temperature difference ΔT , at $T_c = 300$ K. $L = 0.05$ cm, $r_c = 5 \times 10^{-6} \Omega \text{ cm}^2$ (solid lines), $r_c = 10^{-7} \Omega \text{ cm}^2$ (dashed lines), insulating plates: 1— Al_2O_3 , 2—AlN. 3—dependence $\eta_0(\Delta T)$ for the ideal model of module.

Table 6. Ratio of efficiencies η_0/η_{max} and of power densities w_0/w depending on thermoelement length.

Leg Length L , cm	$r_c = 10^{-7} \Omega \text{ cm}^2$, AlN Insulating Plate		$r_c = 10^{-7} \Omega \text{ cm}^2$, Al_2O_3 Insulating Plate		$r_c = 5 \times 10^{-6} \Omega \text{ cm}^2$, AlN Insulating Plate		$r_c = 5 \times 10^{-6} \Omega \text{ cm}^2$, Al_2O_3 Insulating Plate	
	η_0/η_{max}	w_0/w	η_0/η_{max}	w_0/w	η_0/η_{max}	w_0/w	η_0/η_{max}	w_0/w
Temperature difference across a module $\Delta T = 10$ K, $\eta_0 = 0.4838$								
0.2	1.12	1.14	1.14	1.19	1.19	1.22	1.2	1.27
0.1	1.13	1.15	1.17	1.23	1.26	1.32	1.3	1.42
0.05	1.14	1.18	1.23	1.35	1.4	1.52	1.5	1.74
0.025	1.17	1.24	1.35	1.615	1.7	1.96	1.93	2.49
Temperature difference across a module $\Delta T = 25$ K, $\eta_0 = 1.1946$								
0.2	1.05	1.06	1.07	1.1	1.11	1.14	1.13	1.17
0.1	1.06	1.07	1.1	1.15	1.17	1.22	1.21	1.31
0.05	1.07	1.1	1.14	1.25	1.3	1.41	1.39	1.6
0.025	1.1	1.15	1.25	1.48	1.56	1.79	1.76	2.26
Temperature difference across a module $\Delta T = 100$ K, $\eta_0 = 4.3363$								
0.2	1.02	1.02	1.03	1.06	1.06	1.08	1.08	1.12
0.1	1.02	1.03	1.05	1.1	1.11	1.16	1.15	1.23
0.05	1.03	1.06	1.1	1.2	1.21	1.3	1.28	1.47
0.025	1.06	1.1	1.18	1.4	1.42	1.61	1.58	2.02
Temperature difference across a module $\Delta T = 100$ K, $\eta_0 = 4.3363$								
0.2	1.01	1.02	1.02	1.05	1.05	1.07	1.06	1.1
0.1	1.02	1.03	1.04	1.1	1.09	1.12	1.12	1.2
0.05	1.03	1.05	1.08	1.19	1.16	1.25	1.23	1.41
0.025	1.04	1.1	1.15	1.4	1.33	1.5	1.47	1.89

It can be seen that the efficiency η_{max} approaches the value η_0 for the modules with the contact resistivity of $10^{-7} \Omega \text{ cm}^2$ and insulating plates made of AlN. Otherwise η_{max} of the miniscale converters is 1.5–2 times less than the value of η_0 . The power density w is 2.0–2.5 times less than its ideal value w_0 .

For the generating converter, as well as for the cooling module, there is a rational value $r_{c \text{ opt}}$ of the contact resistance, such that for $r_c < r_{c \text{ opt}}$ the increase in the efficiency does not exceed 5%. Figure 15 shows the dependences of $\eta_{max}(r_c)$, which were used to determine the values of $r_{c \text{ opt}}$ for generator converters with different leg lengths. The results are presented in Table 7.

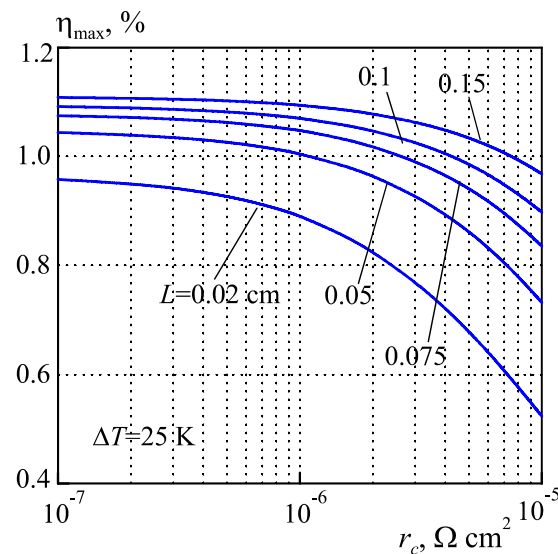


Figure 15. Dependences of maximum efficiency η_{max} on the contact resistivity r_c for different leg length L . $\Delta T = 25 \text{ K}$, insulating plates made of Al_2O_3 .

Table 7. The rational values of the contact resistivity for generating converters with different leg lengths.

Thermoelement length $L, \text{ cm}$	0.15	0.1	0.075	0.05	0.02
Rational contact resistivity $r_{c \text{ opt}}, \Omega \cdot \text{cm}^2$	$3 \cdot 10^{-6}$	$2 \cdot 10^{-6}$	$1.5 \cdot 10^{-6}$	10^{-6}	$6 \cdot 10^{-7}$

These contact resistance values should be adhered to when developing the technology of miniscale generator modules.

It should be noted that the calculated rational values of the contact resistivity, which for miniscale converters with leg lengths from 0.05 cm to 0.02 cm are in the range from $10^{-6} \Omega \cdot \text{cm}^2$ to $3 \cdot 10^{-7} \Omega \cdot \text{cm}^2$, correlate well with the experimental values given in [51] and shown in Table 2. The technology for the fabrication of such contacts is described in detail in [51]. The manufacturing technique of miniscale modules with legs from 0.05 cm to 0.02 cm long has also been developed [49]. It is similar to the technology of modules with traditional leg lengths from 0.1 cm to 0.2 cm. Therefore, it can be confidently stated that there are no obstacles to the mass production of highly efficient miniature converters. The COP or efficiency of such converters will not be less than that of modules with traditional leg lengths. However, the consumption of thermoelectric materials for them will be significantly less, which makes them cheaper.

5. Conclusions

According to the results of the investigation, the following conclusions can be drawn:

- A new numerical method is proposed for designing cooling modules in the maximum COP mode and generating modules with maximum efficiency, with regard to the electrical and thermal resistances of contacts, interconnectors, insulating plates and other factors. The negative effect of these undesirable resistances on the performance of miniscale converters has been estimated. The results prove that the electrical contact resistance becomes the predominant reason for the decrease in the efficiency of converters at the miniaturization of thermoelements.
- A commercial Bi₂Te₃-based module has insulating plates made of Al₂O₃ material and a contact resistivity of about $5 \times 10^{-6} \Omega \text{ cm}^2$. The maximum COP of such a cooling module with a leg length of 0.02 cm is about 2–6 times (depending on temperature drop) less than its possible value for the ideal model of the module (without undesirable electrical and thermal resistances). The efficiency of such modules for generators is about 1.5–2 times less as compared to the ideal model.
- An improvement in the energy efficiency of miniature modules is achieved by decreasing the undesirable resistances to their limit values. Such a limit for the electrical contact resistance is its rational value, which depends on thermoelement length. The rational values for the Bi₂Te₃-based modules both for cooling and generation have been determined and are given in this paper. For miniscale converters with leg lengths from 0.05 cm to 0.02 cm, they vary in the range from $10^{-6} \Omega \cdot \text{cm}^2$ to $3 \cdot 10^{-7} \Omega \cdot \text{cm}^2$ and correlate well with the experimental data obtained in [51]. It is expedient to follow these rational values of contact resistance in the fabrication of miniature modules. To reduce the undesirable thermal resistance, it is preferable to use AlN ceramics instead of insulating plates made of Al₂O₃.

Author Contributions: Conceptualization, L.V.; methodology, L.V.; investigation, L.V.; formal analysis, L.V.; visualization, L.V.; data curation, L.V.; writing—original draft preparation, L.V.; writing—review and editing, L.V.; software, M.K.; validation, M.K. All authors have read and agreed to the published version of the manuscript.

Funding: This paper is part of a research project funded by the National Academy of Sciences of Ukraine (project number 0122U000410).

Data Availability Statement: The data used in this manuscript are available upon reasonable request from the corresponding author.

Acknowledgments: The authors thank the Academician of the National Academy of Sciences of Ukraine Anatyshuk L.I. for fruitful discussions of the research results.

Conflicts of Interest: The authors declare no conflict of interest.

References

1. Champier, D. Thermoelectricity Engineering (Modules, Performance, Applications). 2019. Available online: <https://hal.archives-ouvertes.fr/hal-02367539> (accessed on 23 March 2023).
2. Thermoelectric Modules Market. Available online: <https://www.maximizemarketresearch.com/market-report/thermoelectric-modules-market/2622/> (accessed on 23 March 2023).
3. Dzumedzey, R.O.; Boryk, V.V. Performance specifications of thermoelectric modules on the example of the system “solar collector–thermoelectric generator”. *Phys. Chemistry Solid State* **2013**, *14*, 659–661. Available online: <http://page.if.ua/uploads/pccs/vol14/11403-35.pdf> (accessed on 23 March 2023).
4. Selenium and Tellurium Statistics and Information. Available online: <https://www.usgs.gov/centers/national-minerals-information-center/selenium-and-tellurium-statistics-and-information> (accessed on 23 March 2023).
5. Zhao, D.; Tan, G. A review of thermoelectric cooling: Materials, modeling and applications. *Appl. Therm. Eng.* **2014**, *66*, 15–24. [CrossRef]
6. Nolas, G.S.; Morelli, D.T.; Tritt, T.M. Skutterudites: A phonon-glass-electron crystal approach to advanced thermoelectric energy conversion applications. *Annu. Rev. Mater. Sci.* **1999**, *29*, 89–116. [CrossRef]
7. Shevelkov, A.V.; Kovnir, K. Zintl clathrates. In *Zintl Phases*; Fassler, T.F., Ed.; Springer: Berlin/Heidelberg, Germany, 2011; pp. 97–142. [CrossRef]

8. Shi, X.; Chen, L.; Uher, C. Recent advances in high performance bulk thermoelectric materials. *Int. Mater. Rev.* **2016**, *61*, 379–415. [[CrossRef](#)]
9. Shi, X.; Yang, J.; Salvador, J.R.; Chi, M.; Cho, Y.J.; Wang, H.; Bai, S.; Yang, J.; Zhang, W.; Chen, L. Multiple-filled skutterudites: High thermoelectric figure of merit through separately optimizing electrical and thermal transports. *J. Am. Chem. Soc.* **2011**, *133*, 7837–7846. [[CrossRef](#)] [[PubMed](#)]
10. Morelli, D.T.; Meisner, G.P.; Chen, B.X.; Hu, S.Q.; Uher, C. Cerium filling and doping of cobalt triantimonide. *Phys. Rev. B* **1997**, *56*, 7376–7383. [[CrossRef](#)]
11. Saramat, A.; Svensson, G.; Palmqvist, A.E.C.; Stiewe, C.; Mueller, E.; Platzek, D.; Williams, S.G.K.; Rowe, D.M.; Bryan, J.D.; Stucky, G.D. Large thermoelectric figure of merit at high temperature in Czochralski-grown clathrate $\text{Ba}_8\text{Ga}_{16}\text{Ge}_{30}$. *J. Appl. Phys.* **2006**, *99*, 023708. [[CrossRef](#)]
12. You, S.W.; Shin, D.K.; Ur, S.C.; Kim, I.H. Solid-state synthesis and thermoelectric properties of $\text{Mg}_2\text{Si}_{0.5}\text{Ge}_{0.5}\text{Sb}_m$. *J. Electron. Mater.* **2015**, *44*, 1504–1508. [[CrossRef](#)]
13. Zhang, Q.; He, J.; Zhu, T.J.; Zhang, S.N.; Zhao, X.B.; Tritt, T.M. High figures of merit and natural nanostructures in $\text{Mg}_2\text{Si}_{0.4}\text{Sn}_{0.6}$ based thermoelectric materials. *Appl. Phys. Lett.* **2008**, *93*, 102109. [[CrossRef](#)]
14. Khan, A.U.; Vlachos, N.V.; Hatzikraniotis, E.; Polymeris, G.S.; Lioutas, C.B.; Stefanaki, E.C.; Paraskevopoulos, K.M.; Giapintzakis, I.; Kyratsi, T. Thermoelectric properties of highly efficient Bi-doped $\text{Mg}_2\text{Si}_{1-x-y}\text{Sn}_x\text{Ge}_y$ materials. *Acta Mater.* **2014**, *77*, 43–53. [[CrossRef](#)]
15. Aoyama, I.; Fedorov, M.I.; Zaitsev, V.K.; Solomkin, F.Y.; Eremin, I.S.; Samunin, A.Y.; Mukojima, M.; Sano, S.; Tsuji, T. Effects of Ge doping on micromorphology of MnSi in $\text{MnSi}_{\sim 1.7}$ and on their thermoelectric transport properties. *Jpn. J. Appl. Phys.* **2005**, *44*, 8562–8570. [[CrossRef](#)]
16. Aoyama, I.; Kaibe, H.; Rauscher, L.; Kanda, T.; Mukojima, M.; Sano, S.; Tsuji, T. Doping effects on thermoelectric properties of higher manganese silicides (HMSs, $\text{MnSi}_{1.74}$) and characterization of thermoelectric generating module using p-type (Al, Ge and Mo)-doped HMSs and n-type $\text{Mg}_2\text{Si}_{0.4}\text{Sn}_{0.6}$ legs. *Jpn. J. Appl. Phys.* **2005**, *44*, 4275–4281. [[CrossRef](#)]
17. Pedersen, B.L.; Iversen, B.B. Thermally stable thermoelectric Zn_4Sb_3 by zone-melting synthesis. *Appl. Phys. Lett.* **2008**, *92*, 161907. [[CrossRef](#)]
18. Rhyee, J.-S.; Kim, H. Chemical potential tuning and enhancement of thermoelectric properties in indium selenides. *Materials* **2015**, *8*, 1283–1324. [[CrossRef](#)] [[PubMed](#)]
19. Bottner, H.; Nurnus, J.; Schubert, A. Miniaturized thermoelectric converters. In *Thermoelectrics Handbook: Macro to Nano*; Rowe, D.M., Ed.; Taylor & Francis: London, UK, 2006; pp. 1–16. Available online: <https://www.taylorfrancis.com/chapters/mono/10.1201/9781420038903-46/miniaturized-thermoelectric-converters-rowe> (accessed on 23 March 2023).
20. Sarbu, I.; Dorca, A. A comprehensive review of solar thermoelectric cooling systems. *Int. J. Energy Res.* **2018**, *42*, 395–415. [[CrossRef](#)]
21. Salah, W.A.; Abuhelwa, M. Review of thermoelectric cooling devices recent applications. *J. Eng. Sci. Technol.* **2020**, *15*, 455–476.
22. Sharp, J.; Bierschenk, J.; Lyon, H.B. Overview of solid-state thermoelectric refrigerators and possible applications to on-chip thermal management. *Proc. IEEE* **2006**, *94*, 1602–1612. [[CrossRef](#)]
23. Redmond, M.; Kumar, S. Optimization of thermoelectric coolers for hotspot cooling in three-dimensional stacked chips. *J. Electron. Packag.* **2015**, *137*, 011006. [[CrossRef](#)]
24. Bar-Cohen, A.; Wang, P. On-chip hot spot remediation with miniaturized thermoelectric coolers. *Microgravity Sci. Technol.* **2009**, *21* (Suppl. S1), S351–S359. [[CrossRef](#)]
25. Wang, J.; Zhao, X.-J.; Cai, Y.-J.; Zhang, C.; Bao, W.-W. Experimental study on the thermal management of high-power LED headlight cooling device integrated with thermoelectric cooler package. *Energy Convers. Manag.* **2015**, *101*, 532–540. [[CrossRef](#)]
26. Li, J.; Ma, B.; Wang, R.; Han, L. Study on a cooling system based on thermoelectric cooler for thermal management of high-power LEDs. *Microelectron. Reliab.* **2011**, *51*, 2210–2215. [[CrossRef](#)]
27. Qin, H.; Zhong, D.; Wang, C.H. Thermal performance evaluation and economic analysis of LED integrated with thermoelectric cooler package. *Adv. Mater. Res.* **2011**, *216*, 106–110. [[CrossRef](#)]
28. Shen, L.; Chen, H.; Xiao, F.; Yang, Y.; Wang, S. The step-change cooling performance of miniature thermoelectric module for pulse laser. *Energy Convers. Manag.* **2014**, *80*, 9–45. [[CrossRef](#)]
29. Zhang, W.; Shen, L.; Yang, Y.; Chen, H. Thermal management for a micro semiconductor laser based on thermoelectric cooling. *Appl. Therm. Eng.* **2015**, *90*, 664–673. [[CrossRef](#)]
30. Piotrowski, A.; Piotrowski, J.; Gawron, W.; Pawluczyk, J.; Pedzinska, M. Extension of usable spectral range of Peltier cooled photodetectors. *Acta Phys. Pol. A* **2009**, *116*, s52–s55. [[CrossRef](#)]
31. Anatychuk, L.I.; Vikhor, L.M. The limits of thermoelectric cooling for photodetectors. *J. Thermoelectr.* **2013**, *5*, 54–58.
32. Nordin, L.; Muhowski, A.J.; Wasserman, D. High operating temperature plasmonic infrared detectors. *Appl. Phys. Lett.* **2022**, *120*, 101103. [[CrossRef](#)]
33. Parashchuk, T.; Sidorenko, N.; Ivantsov, L.; Sorokin, A.; Maksymuk, M.; Dzundza, B.; Dashevsky, Z. Development of a solid-state multi-stage thermoelectric cooler. *J. Power Sources* **2021**, *496*, 229821. [[CrossRef](#)]
34. Vullers, R.J.M.; Schaijk, R.; Visser, H.J.; Penders, J.; Hoof, C.V. Energy Harvesting for Autonomous Wireless Sensor Networks. *IEEE Solid State Circuits Mag.* **2010**, *2*, 29–38. [[CrossRef](#)]

35. Dunham, M.T.; Barako, M.T.; LeBlanc, S.; Asheghi-Roudheni, M.; Chen, B.; Goodson, K. Modeling and Optimization of Small Thermoelectric Generators for Low-Power Electronics. In Proceedings of the ASME 2013 International Technical Conference and Exhibition on Packaging and Integration of Electronic and Photonic Microsystems, Burlingame, CA, USA, 16–18 July 2013; Volume 1. [CrossRef]
36. Parsonnet, V. A Lifetime Pacemaker Revisited. *N. Engl. J. Med.* **2007**, *357*, 2638–2639. [CrossRef]
37. Scott, A.; Whalen, C.A.; Apblett, T.L. Improving power density and efficiency of miniature radioisotopic thermoelectric generators. *J. Power Sources* **2008**, *180*, 657–663. [CrossRef]
38. Leonov, V.; Vullers, R. Wearable electronics self-powered by using human body heat: The state of the art and the perspective. *J. Renew. Sustain. Energy* **2009**, *1*, 62701. [CrossRef]
39. Hong, S.; Gu, Y.; Seo, J.K.; Wang, J.; Liu, P.; Shirley Meng, Y.; Xu, S.; Chen, R. Wearable thermoelectrics for personalized thermoregulation. *Sci. Adv.* **2019**, *5*, eaaw0536. [CrossRef]
40. Wei, R.; Sun, Y.; Zhao, D.; Aili, A.; Zhang, S.; Shi, C.; Zhang, J.; Geng, H.; Zhang, J.; Zhang, L.; et al. High-performance wearable thermoelectric generator with self-healing, recycling, and Lego-like reconfiguring capabilities. *Sci. Adv.* **2021**, *7*, eabe0586. [CrossRef]
41. Torfs, T.; Leonov, V.; Vullers, R. Pulse oximeter fully powered by human body heat. *Sens. Transducers J.* **2007**, *80*, 1230–1238.
42. Van Bavel, M.; Leonov, V.; Yazicioglu, R.F.; Torfs, T.; van Hoof, C.; Posthuma, N.; Vullers, R. Wearable battery-free wireless 2-channel EEG systems powered by energy scavengers. *Sens. Transducers J.* **2008**, *94*, 103–115.
43. Kim, C.S.; Yang, H.M.; Lee, J.; Lee, G.S.; Choi, H.; Kim, Y.J.; Lim, S.H.; Cho, S.H.; Cho, B.J. Self-powered wearable electrocardiography using a wearable thermoelectric power generator. *ACS Energy Lett.* **2018**, *3*, 501–507. [CrossRef]
44. Leonov, V.; Torfs, T.; van Hoof, C.; Vullers, R.J. Smart wireless sensors integrated in clothing: An electrocardiography system in a shirt powered using human body heat. *Sens. Transducers J.* **2009**, *107*, 165.
45. Vondrak, J.; Schmidt, M.; Proto, A.; Penhaker, M.; Jargus, J.; Peter, L. Using Miniature Thermoelectric Generators for Wearable Energy Harvesting. In Proceedings of the 2019 4th International Conference on Smart and Sustainable Technologies (SpliTech), Split, Croatia, 18–21 June 2019; pp. 1–6. [CrossRef]
46. Xu, Q.; Deng, B.; Zhang, L.; Lin, S.; Han, Z.; Zhou, Q.; Li, J.; Zhu, Y.; Jiang, F.; Li, Q.; et al. High-performance, flexible thermoelectric generator based on bulk materials. *Cell Rep. Phys. Sci.* **2022**, *3*, 100780. [CrossRef]
47. Bahk, J.-H.; Fang, H.; Yazawa, K.; Shakouri, A. Flexible thermoelectric materials and device optimization for wearable energy harvesting. *J. Mater. Chem. C* **2015**, *3*, 10362–10374. [CrossRef]
48. Du, Y.; Xu, J.; Paul, B.; Eklund, P. Flexible thermoelectric materials and devices. *Appl. Mater. Today* **2018**, *12*, 366–388. [CrossRef]
49. Semenyuk, V.A. Thermoelectric Cooling of Electro-Optic Components. In *Thermoelectrics Handbook: Macro to Nano*; Rowe, D.M., Ed.; Taylor & Francis: London, UK, 2006; pp. 1–20. [CrossRef]
50. Anatyshuk, L.I. *Thermoelectricity. Volume 2. Thermoelectric Energy Convertors*; Institute of Thermoelectricity: Chernivtsi, Ukraine, 2003; Available online: <http://library.lol/main/9D47871457FBA3B0F47B88ACB76589E1> (accessed on 23 March 2023).
51. Taylor, P.J.; Maddux, J.R.; Meissner, G.; Venkatasubramanian, R.; Bulman, G.; Pierce, J.; Gupta, R.; Bierschenk, J.; Caylor, C.; D'Angelo, J.; et al. Controlled improvement in specific contact resistivity for thermoelectric materials by ion implantation. *Appl. Phys. Lett.* **2013**, *103*, 043902. [CrossRef]
52. Ioffe, A.F. *Semiconductor Thermoelements and Thermoelectric Cooling*; Infoserch Limited: London, UK, 1957; Available online: <http://library.lol/main/957FA64C64DACD34F22E31B2035B549B> (accessed on 23 March 2023).
53. Chen, L.; Mei, D.; Wang, Y.; Li, Y. Ni barrier in Bi₂Te₃-based thermoelectric modules for reduced contact resistance and enhanced power generation properties. *J. Alloys Compd.* **2019**, *796*, 314–320. [CrossRef]
54. Joshi, G.; Mitchell, D.; Ruedin, J.; Hoover, K.; Guzman, R.; McAleer, M.; Wood, L.; Savoy, S. Pulsed-light surface annealing for low contact resistance interfaces between metal electrodes and bismuth telluride thermoelectric materials. *J. Mater. Chem. C* **2019**, *7*, 479–483. [CrossRef]
55. Gupta, R.P.; Xiong, K.; White, J.B.; Cho, K.; Alshareef, H.N.; Gnade, B.E. Low Resistance Ohmic Contacts to Bi₂Te₃ Using Ni and Co Metallization. *J. Electrochem. Soc.* **2010**, *157*, H666. [CrossRef]
56. Gupta, R.P.; McCarty, R.; Sharp, J. Practical contact resistance measurement method for bulk Bi₂Te₃ based thermoelectric devices. *J. Electron. Mater.* **2014**, *43*, 1608–1612. [CrossRef]
57. Kuznetsov, G.D.; Polystanskiy, Y.G.; Evseev, V.A. The metallization of the thermoelement branches by ionic sputtering of the nickel and cobalt. In Proceedings of the XIV International Conference on Thermoelectrics, St. Petersburg, Russia, 27–30 June 1995; pp. 166–167. Available online: https://books.google.com.ua/books/about/Proceedings_of_the_XIV_International_Con.html?id=P7jrAQAACAAJ&redir_esc=y (accessed on 23 March 2023).
58. Vikhor, L.M.; Anatyshuk, L.I.; Gorskyi, P.V. Electrical resistance of metal contact to Bi₂Te₃ based thermoelectric legs. *J. Appl. Phys.* **2019**, *126*, 164503. [CrossRef]
59. Gupta, R.; White, J.; Iyore, O.; Chakrabati, U.; Alshareef, H.; Gnade, B. Determination of contact resistivity by the Cox and Strack method for metal contacts to bulk bismuth antimony telluride. *Electrochem. Solid State Lett.* **2009**, *12*, H302–H304. [CrossRef]
60. Min, G.; Rowe, D.M. Improved model for calculating the coefficient of performance of a Peltier module. *Energy Convers. Manag.* **2000**, *41*, 163–171. [CrossRef]
61. Xuan, X.C. Investigation of thermal contact effect on thermoelectric coolers. *Energy Convers. Manag.* **2003**, *44*, 399–410. [CrossRef]

62. Gou, X.; Xiao, H.; Yang, S. Modeling, experimental study and optimization on low-temperature waste heat thermoelectric generator system. *Appl. Energy* **2010**, *87*, 3131–3136. [[CrossRef](#)]
63. Shen, Z.-G.; Wu, S.-Y.; Xiao, L.; Yin, G. Theoretical modeling of thermoelectric generator with particular emphasis on the effect of side surface heat transfer. *Energy* **2016**, *95*, 367–379. [[CrossRef](#)]
64. He, H.; Liu, W.; Wu, Y.; Rong, M.; Zhao, P.; Tang, X. An approximate and efficient characterization method for temperature-dependent parameters of thermoelectric modules. *Energy Convers. Manag.* **2019**, *180*, 584–597. [[CrossRef](#)]
65. He, H.; Wu, Y.; Liu, W.; Rong, M.; Fang, Z.; Tang, X. Comprehensive modeling for geometric optimization of a thermoelectric generator module. *Energy Convers. Manag.* **2019**, *183*, 645–659. [[CrossRef](#)]
66. Montecucco, A.; Buckle, A.R.; Knox, V. Solution to the 1-D unsteady heat conduction equation with internal Joule heat generation for thermoelectric devices. *Appl. Thermal Eng.* **2012**, *35*, 177–184. [[CrossRef](#)]
67. Huang, M.-J.; Yen, R.-H.; Wang, A.-B. The influence of the Thomson effect on the performance of a thermoelectric cooler. *Int. J. Heat Mass Transfer.* **2005**, *48*, 413–418. [[CrossRef](#)]
68. Meng, F.; Chen, L.; Sun, F. A numerical model and comparative investigation of a thermoelectric generator with multi-irreversibilities. *Energy* **2011**, *36*, 3513–3522. [[CrossRef](#)]
69. Chen, W.-H.; Liao, C.-Y.; Hung, C.-I. A numerical study on the performance of miniature thermoelectric cooler affected by Thomson effect. *Appl. Energy* **2012**, *89*, 464–473. [[CrossRef](#)]
70. Zhu, W.; Deng, Y.; Wang, Y.; Wang, A. Finite element analysis of miniature thermoelectric coolers with high cooling performance and short response time. *Microelectron. J.* **2013**, *44*, 860–868. [[CrossRef](#)]
71. Wang, X.-D.; Huang, Y.-X.; Cheng, C.-H.; Lin, D.T.-W.; Kang, C.-H. A three-dimensional numerical modeling of thermoelectric device with consideration of coupling of temperature field and electric potential field. *Energy* **2012**, *47*, 488–497. [[CrossRef](#)]
72. Jang, B.; Han, S.; Kim, J.-Y. Optimal design for micro-thermoelectric generators using finite element analysis. *Microelectron. Eng.* **2011**, *88*, 775–778. [[CrossRef](#)]
73. Wang, X.; Qi, J.; Deng, W.; Li, G.; Gao, X.; He, L.; Zhang, S. An optimized design approach concerning thermoelectric generators with frustum-shaped legs based on three-dimensional multiphysics model. *Energy* **2021**, *233*, 120810. [[CrossRef](#)]
74. Anatyshuk, L.I.; Havrylyuk, N.V.; Lysko, V.V. Methods and equipment for quality control of thermoelectric materials. *J. Electron. Mater.* **2012**, *41*, 1680–1685. [[CrossRef](#)]
75. Anatyshuk, L.I.; Havrylyuk, N.V.; Lysko, V.V. Absolute method for measuring of thermoelectric properties of materials. *Mater. Today Proc.* **2015**, *2*, 737–743. [[CrossRef](#)]
76. Anatyshuk, L.I.; Vikhor, L.M.; Mitskaniuk, N.V. Contact resistance due to potential barrier at thermoelectric material–metal boundary. *J. Thermoelectr.* **2019**, *4*, 74–88.

Disclaimer/Publisher’s Note: The statements, opinions and data contained in all publications are solely those of the individual author(s) and contributor(s) and not of MDPI and/or the editor(s). MDPI and/or the editor(s) disclaim responsibility for any injury to people or property resulting from any ideas, methods, instructions or products referred to in the content.